The Gantry-Tau – Summary of Latest Development at ABB, University of Agder and University of Queensland.

Geir Hovland and Martin Choux, University of Agder, Grimstad, Norway
Matthew Murray and Ilya Tyapin, University of Queensland, Australia
Torgny Brogårdh, ABB Robotics, Västerås, Sweden

Abstract

The Gantry-Tau is a PKM structure having a large accessible work space in relation to its footprint. In this paper some of the features of the Gantry-Tau structure will be described and a summary of some results will be presented from the analysis of the kinematic, elastostatic and elastodynamic properties of the PKM. In the case of kinematics a 5 axes Gantry-Tau will be described as well as methods for the calibration and reconfiguration of the structure. For the elastostatic and elastodynamic analysis a method assuming that each PKM link can be described as a mass-spring-damper model will be presented. A new design optimisation scheme taking the kinematic and elastostatic properties into account will also summarized.

1. Introduction

The Gantry-Tau parallel kinematic machine (PKM) has a non-symmetric link structure with its arms built up from 3, 2 and 1 links respectively. This non-symmetric link arrangement has shown to give several important features. Some of these features can be observed from Fig. 1: 1) A large accessible work space is obtained. 2) It is possibility to use a thin platform carrying the tool, whereby almost the full space between LM2 and LM3 can be used. 3) The option to introduce a redundant telescopic linear actuator in the single link LR1 will increase the stiffness significantly since the single link can be controlled to have a favourable angle relative the platform. 3) Increasing the distances between the links LR1/LR2 and between the links LR4/LR6 will increase the stiffness with respect to platform torques without reducing the work space between LM2 and LM3.

Proceedings of the *the 3rd Intl. Colloquium: Robotic Systems for Handling and Assembly*, the Collaborative Research Centre SFB 562, Braunschweig, Germany, April 2008.

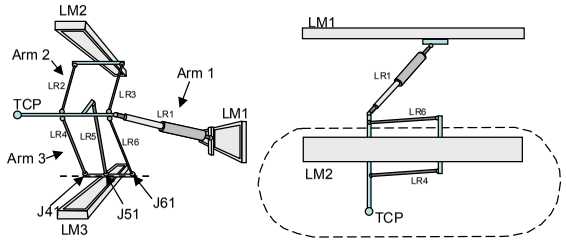

Figure 1: The reconfigurable Gantry-Tau PKM as seen from the front and from above. The link rods LR1 – LR6 are actuated by the linear modules LM1 – LM3. The link LR1 is here implemented as a linear telescope actuator. The joints J41, J51 and J61 are mounted along a horizontal line to make reconfiguration possible.

The reconfigurable Gantry-Tau structure is investigated both theoretically and experimentally in research collaboration between ABB Robotics and the Universities of Agder and Queensland. Thus, the kinematics of a 5 DOF Gantry-Tau has been obtained and a calibration method for the 3 DOF version of the manipulator has been developed. Moreover, a method for deriving the elastostatic properties has been found and it has been shown that the link forces used for the calculations of the elastostatics also can be used to calculate singularity free paths for the reconfiguration of a 5 DOF Gantry-Tau manipulator. The elastodynamic property of the manipulator has been found and a geometric design optimization method has been developed. In this paper a short summary of this work will be presented. The reconfiguration work in section 5 is presented for the first time in this paper.

2. Five DOF Kinematics

Five DOF manipulation using the Gantry-Tau was achieved by modifying the arm structure in such a way that two linear telescope link actuators were introduced, for example to control the lengths of links LR3 and LR6 in Fig. 1. For the derivation of the 5 DOF inverse kinematics, the notations in Fig.2 (left) were used. The controlled variables are the linear actuator positions q_1, q_2, q_3 together with the link lengths q_4 and q_5.

Fig. 2 (right) shows the manipulated platform used in the derivation. This platform is larger than in Fig. 1, which depends on the design, where a spindle is integrated into the platform. The platform points A to F in Fig. 2 (right) were calculated in the global coordinate system. The two rotational platform angles r_x and r_z (rotational angles around the TCP X- and Z-axes in Figure 3) can be specified to achieve 5-DOF together with the TCP position X,Y,Z. In order to solve the inverse kinematics the dependent platform rotation r_y caused by the triangularly mounted links of arm 3 was solved first. The drive variable q_3 could then be eliminated using a Weierstrass substitution. Once the tool platform rotation r_Y was determined the position of all joints connected to the tool platform could be calculated. The drive positions q_3, q_1 and q_2 were then determined and the lengths of the telescopic links q_4 and q_5 were found by simply calculating the distances between the respective links joints on the platform and the guide ways. The derivation and the analytical expressions for the inverse kinematics are too complex to show here.

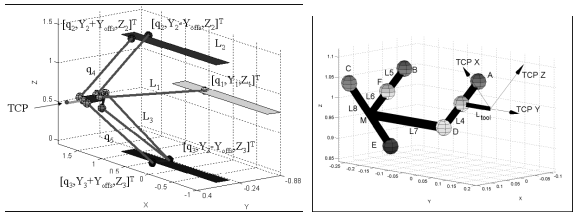

Figure 2: (Left) Gantry-Tau shown in the left-handed configuration for all links. (Right) Definition of the geometry of the manipulated platform. A-F are the joints on the platform.

Besides using the 5 DOF inverse kinematics for the control of the Gantry-Tau robot at UiA it was also used for designing collision-free 5 DOF actuation. In the left plot in Fig. 4 all 9 combinations of the platform orientations $r_x = 0, -30^o, +30^o$ and $r_z = 0, -30^o, +30^o$ were tested over the whole work space. As can be seen the manipulator only has the possibility to obtain all the platform orientations without collisions in work space islands, marked by "1" in the figure (grey areas indicate collisions between links or between links and platform).

By changing the relative positions of the joints on the platform (A –F in Fig. 2 (right)) the collision free work space areas could be increased. Thus, the right plot in Fig. 3 shows the result of a platform joint layout where almost the whole Gantry-Tau workspace can be used for platform rotations of ±30 degrees. It should be mentioned that with this design the maximum allowable platform rotations will increase (be larger than ±30 degrees) the closer to the centre of the work space the manipulated platform is.

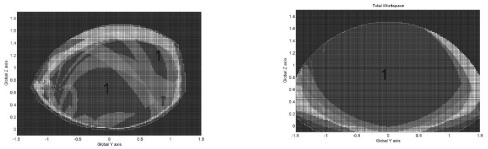

Figure 3: (Left) Work space study of the 5 DOF manipulator with requirements on platform rotations of ±30 degrees. Only the darker areas (indicated with the number 1) are able to fulfil the requirements. (Right) Improvement of the area (1) where platform rotations of ±30 degrees can be made. This is obtained by optimizing the positions of the platform joints.

3. Calibration

In order to minimize the installation cost of the reconfigurable Gantry-Tau robot it would have been a big advantage if it was possible to mount the linear guide ways without the precision needed for a serial Gantry manipulators used in industry today. Since the mechanically not redundant arm structure does not require that the linear guide ways are mounted in parallel this should actually be possible. However, the kinematics of the robot will of course depend on the geometry of the mounting of the guide ways. It is therefore necessary to find the kinematics of the Gantry-Tau when the guide ways are not parallel and make use of the obtained kinematics during calibration of the manipulator.

Fig. 4 shows a drawing of the Gantry-Tau with not parallel guide ways. When deriving the inverse kinematics the track positions for the first and second arms (see definitions in Fig. 1) were quite easy to calculate also in this case but the calculations of the track position of the third arm became more complex.

For the third arm a quadratic equation was achieved, which could be solved with an analytic solution [2, 3]. From this solution the third track position q_3 could be

calculated and the track positions q_1 and q_2 for the first and second arm were found by setting up the equations for a sphere and a line [4]. These computations yielded the inverse kinematics of the Gantry-Tau for not parallel linear actuators.

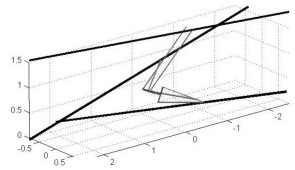

Figure 4: The Gantry-Tau with not parallel guide ways.

With the inverse kinematics available, it was possible to identify the error parameters for the track mountings, which means performing an optimization to obtain a best fit between a set of kinematics error parameters and measurement data when the manipulator is in different configurations. If an accurate 3D Measurement System is available, positions of the manipulated platform can be collected in the whole work space. Simultaneously the positions of the arms on the guide ways can be obtained from the manipulator controller. The measured positions of the platform (*x, y, z*) are then used in the kinematic model to calculate the positions of the arms on the guide ways (q_1, q_2, q_3) and doing so for a number of positions in the work space the error parameters can be calculated.

To verify the identification concept simulations were made with 3 different measurement concepts: Using a 3D measurement system, using a 1D measurement system measuring along a line and using a 1D measurement system measuring along a circle arc. In the identification simulations the following error parameters for the guide ways were selected (rad and m): $\theta_1 = 0.025$, $\varphi_1 = 0.023$, $y_{error1} = 0.2$, $z_{error1} = 0.01$, $\theta_2 = 0$, $\varphi_2 = 0.04$, $y_{error2} = 0.01$, $z_{error2} = 0.05$, $\theta_3 = 0.1$, $\varphi_3 = 0.02$, $y_{error3} = 0.0015$ and $z_{error3} = 0.005$. By means of SVD analysis the best 50 manipulator configurations were selected for identification, which gave the identification results shown in Table 1. As can be seen the best identification was obtained when using 3D measurements, whereby the measurement points can be deployed anywhere in the work space. "Oblique" means 1D measurements with for example a linear encoder parallel with the guide ways and "Two linear" means that

2 linear encoders are mounted perpendicular to the guide ways. In the case "Dbb" a double ball bar is used. The calibration simulation was made by inserting the identified parameters into the kinematic model used to control the simulated manipulator.

Parameter	3D	Oblique	Two linear	Dbb
θ_1	0.0250	−0.0036	0.0245	0.0250
ϕ_1	0.0230	0.0560	0.0230	0.0230
y_{error1}	0.2000	0.1206	0.1991	0.2000
z_{error1}	0.0100	0.1126	0.0099	0.0100
$theta_2$	0.0000	0.0251	0.0000	0.0000
ϕ_2	0.0400	0.0089	0.0400	0.0400
y_{error2}	0.0100	0.0255	0.0100	0.0100
z_{error2}	0.0500	0.0062	0.0500	0.0500
θ_3	0.1000	0.0993	0.1001	0.1000
ϕ_3	0.0200	0.0204	0.0200	0.0199
y_{error3}	0.0015	−0.0014	0.0017	0.0014
z_{error3}	0.0050	0.0059	0.0050	0.0049
RMS error 10^{-3}	0.0000	0.7500	0.1000	0.0250

Table 1: Results of the simulation of manipulator error identification using different measurement concepts.

4. Elastostatic Analysis

An elastostatic analysis was made for the reconfigurable Gantry-Tau. In the analysis X, Y, Z are the TCP coordinates, α, β, γ the TCP orientation angles and l_i and F_i (i = 1, · · · , 6) the six PKM link lengths and link forces. F_x, F_y and F_z are the external Cartesian forces and M_x, M_y and M_z are the external Cartesian torques acting on the TCP. The following vectors can then be introduced:

$$\mathbf{X} = [X\ Y\ Z]^T;\ \ \theta = [\alpha\ \beta\ \gamma]^T\ ;\ \mathbf{F} = [F_x\ \ F_y\ \ F_z]^T\ ;\ \mathbf{M} = [M_x\ \ M_y\ \ M_z]^T$$

$$\mathbf{L} = [l_1\ \ l_2\ \ l_3\ \ l_4\ \ l_5\ \ l_6]^T;\ \mathbf{F}_a = [F_1\ \ F_2\ \ F_3\ \ F_4\ \ F_5\ \ F_6]^T$$

The relationships between the TCP forces and the link forces are given by the first two equations below:

$$\mathbf{F} = \sum_{i=1}^{6} F_i \mathbf{u}_i \qquad \mathbf{M} = \sum_{i=1}^{6} F_i \mathbf{A}_i \times \mathbf{u}_i \qquad \begin{bmatrix} \mathbf{F} \\ \mathbf{M} \end{bmatrix} = \mathbf{H}\mathbf{F}_a \qquad \begin{bmatrix} \Delta\mathbf{X} \\ \Delta\theta \end{bmatrix} = \mathbf{J}\Delta\mathbf{L} \quad (1)$$

where u_i is a unit vector in the direction of link i and A_i is a vector pointing from the TCP to the platform-side end-point of link i. The two equations (above left) were rewritten using the 6 × 6 statics matrix H (above right).

The Jacobian matrix **J** introduced above relates changes in Cartesian position and orientation (ΔX and $\Delta\theta$) to changes in the link lengths (ΔL). Gosselin [5] showed the duality between the statics and the link Jacobian for PKMs, giving the following equality: $\mathbf{H}^{-1} = \mathbf{J}^{T}$. Based on this duality result, the Cartesian stiffness matrix *K* was derived as $\mathbf{K} = \mathbf{H}\mathbf{K}_L\mathbf{H}^{T}$, where $\mathbf{K}_L$ is a 6 × 6 diagonal matrix with the individual link stiffness along the diagonal.

The PKM stiffness was calculated for forces on the TCP in different directions and in different positions in the work space. These calculations were made for the reconfigurable Gantry-Tau, which had 5 fixed links lengths of 1.0 m and one single telescopic actuator link as was illustrated in Fig. 1. The Cartesian X-positions of the arm mountings on the linear guide ways are q_1, q_2 and q_3 as illustrated in Fig. 2 while the Y- and Z-coordinates of the guide ways are fixed and are given by: $Y_1 = -Q$, $Z_1 = Q$, $Y_2 = 0$, $Z_2 = 2Q$, $Y_3 = 0$ and $Z_3 = 0$, where $Q = 0.5$ m. The telescopic link length was actively controlled such that $q_1 = X$ where possible, which gave favourable angles between the single link and the other links in most of the work space. Each of the 12 universal joints had a stiffness of 50 N/µm and the link rods had the stiffness 232 N/ µm (all values as in the prototype at University of Agder). The stiffness of the support frame and the actuators were assumed to be infinite. The calculated minimum, maximum and average Cartesian stiffness values of the telescopic version of the PKM in the entire workspace and in the best 70% of the workspace are listed in Table 2.

Entire Workspace	**X**	**Y**	**Z**
Minimum	19.50	5.06	18.69
Maximum	67.51	57.88	55.46
Average	53.20	22.28	29.36
Best 70% Workspace	**X**	**Y**	**Z**
Minimum	49.37	13.81	22.55
Maximum	67.51	57.88	55.46
Average	59.13	27.70	33.08

Table 2: Cartesian stiffness values (N/µm) in the X-, Y- and Z-directions of the reconfigurable PKM with telescopic link in arm 1 as shown in Fig 1. The max, min and average values are for the whole and for the best 70% workspace. The border areas of the work space have been removed in the 70% case

5. Reconfiguration using 5 DOF Kinematics

The inverse kinematics (IK) presented in section 2 has two solutions for each of the three base actuators for a fixed TCP position and orientation. Hence, there are in total eight possible solutions for the IK. Each of these solutions is typically called assembly mode in the literature, as in the past the only way to change the mode has been to dismount and re-assemble the PKM. Fig.6 to the left illustrates the two most important assembly modes of the Gantry-Tau, where the arms are mounted either all left or all right with respect to the three base actuators. The two assembly modes to the left in Fig 5 are important because the robot can only reach both workspace extremes in these two modes.

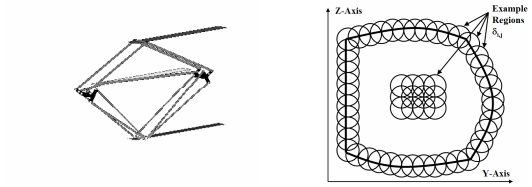

Figure 5: (Left) The two most important assembly modes for Gantry-Tau, all left and all right. (Right) Example of work space spherical regions $\delta_{i,j}$.

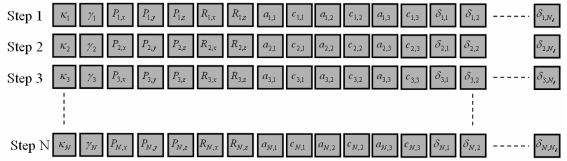

*Figure 6: Illustration of state vector **x**.*

An approach based on Mixed Integer Linear Programming (MILP) optimization [6] was used to determine a near optimal path for automatically reconfiguring the Gantry-Tau PKM while avoiding Type-II singularities. Fig. 5 (right) shows the workspace in the YZ-plane of the Gantry-Tau. This workspace is discretized into

smaller spherical regions named $\delta_{i,j}$. Fig. 6 shows the entire state vector **x** for the optimization problem where the optimized path is discretized into N steps. In addition to the region variables $\delta_{i,j}$, the state vector **x** contains the following variables for each step i: κ_i (condition number of the PKM statics matrix **H** (see eq.(1))), γ_i (boolean help variable to stop optimization when the goal region j_N has been reached), $P_{i,x}$, $P_{i,y}$, $P_{i,z}$, $R_{i,x}$, $R_{i,z}$ (5-DOF TCP position and orientation) and $a_{i,j}$, $c_{i,j}$ (boolean assembly mode and assembly change mode variables for the main actuators j=1,2,3). The path optimization is given by the following objective function and linear constraints.

$$\begin{aligned} &\min \quad \mathbf{g}^T\mathbf{x} \\ &\textit{subject to} \quad \mathbf{Ax} \le \mathbf{B} \end{aligned} \tag{2}$$

The optimization problem was defined in this case as a minimization of the sum of the condition numbers of the PKM matrix **H**, eq.(1), during the reconfiguration path and the objective function vector **g** was found to be: g(k)=1 if $k \in \{1, 13+N_d+1, \ldots, (13+N_d)(N-1)+1\}$ and zero otherwise, where N_d is the total number of regions $\delta_{i,j}$ for one step i. Let j_0 be the initial region and j_N be the final goal region. Then, the following constraints (3 to the left) are required.

$$\begin{aligned} &\delta_{1,j0} = 1 \\ &\delta_{1,j} = 0 \qquad j \ne j_0 \\ &\delta_{N\_j,jN} = 1 \\ &\delta_{N,j} = 0 \qquad j \ne j_N \end{aligned} \qquad\qquad \sum_{j=1}^{N_\delta} \delta_{i,j} = 1 \tag{3}$$

For each step number i only one state $\delta_{i,j}$ can be set to 1, and the constraint in eq.(3 to the right) is required. In order to prevent that the Cartesian distance between two step numbers becomes too large, a new type of constraint based on the TCP coordinates is introduced as follows (4 left).

$$\begin{aligned} &-\Delta X \le P_{x,j} - P_{x,j-1} \le \Delta X \\ &-\Delta Y \le P_{y,j} - P_{y,j-1} \le \Delta Y \\ &-\Delta Z \le P_{z,j} - P_{z,j-1} \le \Delta Z \\ &-\Delta R_x \le R_{x,j} - R_{x,j-1} \le \Delta R_x \\ &-\Delta R_z \le R_{z,j} - R_{z,j-1} \le \Delta R_z \end{aligned} \qquad\qquad \begin{aligned} &IF\ \delta_{i,j} == 1\ THEN\ P_{x,i} = X(j) \\ &IF\ \delta_{i,j} == 1\ THEN\ P_{y,j} = Y(j) \\ &IF\ \delta_{i,j} == 1\ THEN\ P_{z,j} = Z(j) \\ &IF\ \delta_{i,j} == 1\ THEN\ R_{x,j} = R_x(j) \\ &IF\ \delta_{i,j} == 1\ THEN\ P_{z,j} = R_z(j) \end{aligned} \tag{4}$$

The constraints in eqs. (4 left) prevent that the TCP position changes more than the threshold distances ΔX, ΔY, ΔZ between two step numbers. The threshold distances are chosen such that the maximum travelled distance equals the diameter of the region spheres illustrated in Fig.5 (to the right). ΔR_x and ΔR_z are the maximum TCP orientation change values, for examples 5 degrees, between two steps.

To set the TCP positions and orientations for each step number i, the following mixed-integer types of constraints are required. The logical constraint in eq. (4 right) can be implemented by two linear constraints (5 left) as follows.

$$\begin{aligned} &-m\delta_{i,j} + P_{x,j} \le X(j) - m \\ &M\delta_{i,j} - P_{x,j} \le -X(j) + M \end{aligned} \qquad\qquad \begin{aligned} &IF\ \delta_{i,j} == 1 \quad THEN\ \kappa_i = \gamma_i \kappa(j) \\ &IF\ \delta_{i,jN} == 1\ THEN\ \gamma_i = 0 \\ &\qquad\qquad\qquad ELSE \quad \gamma_i = 1 \end{aligned} \tag{5}$$

where m, M are the minimum and maximum values of X(j) respectively, see for example [7] for examples of such logical constraints. The logical constraints in eq.(5 right) ensure that the summation of the condition numbers stops once the final goal region j_N has been reached.

The IF-THEN-ELSE type of logical constraint in eq.(5 right) can be implemented by the following four linear constraints (6 left).

$$\begin{aligned} &0.99\delta_{i,jN} + \gamma_i \le 1 \\ &-1.01\delta_{i,jN} - \gamma_i \le -1 \\ &1.01\delta_{i,jN} + \gamma_i \le 1.01 \\ &-0.99\delta_{i,jN} - \gamma_i \le -0.99 \end{aligned} \qquad\qquad \begin{aligned} &IF\ \delta == 1\ THEN\ z = f_1\ ELSE\ z = f_2 \\ &(m_2 - M_1)\delta + z \le f_2 \\ &(m_1 - M_2)\delta - z \le -f_2 \\ &(M_2 - m_1)\delta + z \le f_1 + (M_2 - m_1) \\ &(M_1 - m_2)\delta - z \le -f_1 + (M_1 - m_2) \end{aligned} \tag{6}$$

The general logical rules for an IF-THEN-ELSE statement are shown in eq. (6 right), where m_1, m_2 and M_1, M_2 are the lower and upper limits on the functions f_1 and f_2, respectively.

$$\begin{aligned} &IF\ \delta_{i,j} == 1\ THEN\ a_{i,k} = A_k(j) \\ &IF\ \delta_{i,j} == 1\ THEN\ c_{i,k} = C_k(j) \\ &IF\ c_{i-1,k} = 0\ THEN\ a_{i,k} = a_{i-1,k} \end{aligned} \tag{7}$$

The first two logical constraints in eq.(7) set the current assembly mode and the assembly mode change variables equal to the corresponding values for the active

region $\delta_{i,j}$. The third logical constraint in eq.(7) sets the current assembly mode for actuator k (k=1, 2, 3) equal to the assembly mode for the previous step, if the change variable equals zero. Hence, the assembly mode for actuator k is only allowed to change at step i if the change variable $c_{i-1,k}$ is equal to 1. In order to formulate the entire MILP optimization problem, an offline pre-processing step is required which associates the following variables with a region j: X(j), Y(j), Z(j), R_x(j), R_z(j), κ(j), A_k(j), C_k(j). C_k(j)=1 represents regions in the workspace for two different assembly modes where the change of actuator k value approaches zero. $A_k(j) \in [0,1]$ represents the assembly mode (left or right) for actuator k for region j.

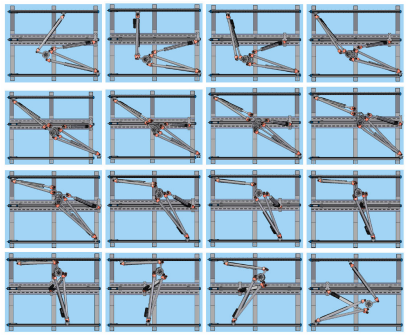

Figure 7: Example of Reconfiguration Sequence on the 5-DOF Gantry-Tau prototype at UiA (sequence moves from left to right and top to bottom).

Fig. 7 shows an example of an optimized path when the actuator lengths are 2.1m, the support frame has depth 0.75m and height 1.5m. The arm lengths are 1.09m for arms 1 and 2, and 1.25m for arm 3.

Fig. 9 shows the optimized path in the YZ-plane of the workspace. The actual path of the TCP is illustrated by the solid red line, while the singularities are marked by the lighter coloured lines. For example step 1 has a singularity-free workspace, while step 2 has a singular area when the TCP has low Y-values and the Z-values are in the middle of the workspace. Note that the X values of the TCP have no influence on the condition number of the statics matrix **H**.

Fig. 8 shows the actual condition number plotted versus the optimization step number i for the path in Figure 9. At singularities, the condition number of the statics matrix **H** approaches infinity, while Fig. 8 shows that the path is well clear of singular points and the maximum condition number is 59.00. The maximum condition takes place at the 5th picture in Figs. 7 and 9. The circled dots in Fig. 8 correspond to the 16 pictures in Figs. 7 and 9. The MILP optimization problem was solved using ILOG CPLEX v11 with a total of N=23 optimization steps and N_d=45,936 region booleans $\delta_{i,j}$ per step. The total number of variables for CPLEX to solve equals $(13+N_d)*N$=1,056,827 and the solution time is about 15 minutes to solve on a standard computer. Fig. 8 illustrates an interpolated path with 220 steps. The 16 pictures in Figs. 7 and 9 illustrate 16 selected steps from the total interpolated path of 220 steps.

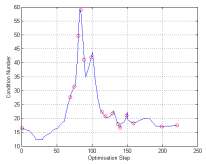

*Figure 8: Condition number of matrix **H** along the optimized reconfiguration path illustrated in Figures 7 and 9.*

6. Elastodynamic Analysis

Beside high stiffness also high mechanical bandwidth is very important, which means that the lowest eigenfrequencies of the manipulator must be high enough to permit high performance control. To calculate the lowest eigenfrequency of the Gantry-Tau a flexible model of the links was used. This model consisted of 2 masses and 2 spring/damper pairs for each link. Isolating the dynamics for link i and then the platform, the flexible equations of motion could be set up. By linearization and introducing the Laplace transform, 18 flexible motion equations could then be written on matrix form (8 left).

$$\begin{bmatrix} A & -B \\ C & D \end{bmatrix} \begin{bmatrix} a_i \\ l_i \end{bmatrix} = \begin{bmatrix} \mathbf{0} \\ \mathbf{F} \\ \mathbf{M} \end{bmatrix} \qquad A = (M_a s^2 + (z_1 + z_2)s + k_1 + k_2)\mathbf{I}_6;\ B = (z_2 s + k_2)\mathbf{I}_6 \qquad (8)$$

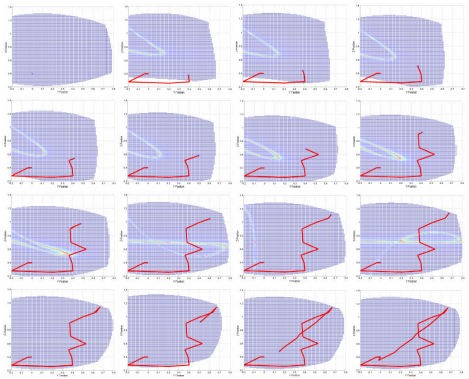

Figure 9: Optimized path (red line) in the YZ-plane with corresponding condition number maps (light blue loops). The sequence moves from left to right and top to bottom and corresponds to Figure 7.

The vector **0** (8 left) is a 6 × 1 zero vector and the matrix elements A, B, C and D are Laplace transform polynomials. $\mathbf{I}_6$ is a 6 × 6 identity matrix (8 right). In addition to the link masses, springs and dampers, the 6×6 sub-matrices C and D will also contain platform parameters, such as the platform weight and inertia. The Cartesian position vector $\mathbf{X}$ and the orientation vector θ were replaced by a and l by using the Jacobian matrix. The 12 unknown parameters a_i and l_i could then be solved by inverting the matrix in eq. (8 left). Knowing the direct link Jacobian matrix of the PKM, the Cartesian velocities could be calculated as follows (9 left):

$$\begin{bmatrix}\mathbf{X}\\ \theta\end{bmatrix} = \mathbf{JL} \;\rightarrow\; s\mathbf{I}_6\begin{bmatrix}\mathbf{X}\\ \theta\end{bmatrix} = s\mathbf{I}_6\mathbf{JL} \qquad \frac{\mathbf{X}_i}{F_j}(s) = \frac{\mathbf{X}_i}{l_i}(s)\frac{l_i}{F_j}(s) \qquad \frac{\theta_i}{M_j}(s) = \frac{\theta_i}{l_i}(s)\frac{l_i}{M_j}(s) \qquad (9)$$

where $L = [l_1, \cdots, l_6]^{\mathrm{T}}$. The final transfer functions of the PKM from Cartesian forces/torques to positions/orientations could then be derived from eq. (9 right 2 expressions).

Using the same stiffness values as in the earlier presented elastostatic calculations, joint weight of 1 kg, link weight of 1kg, a manipulated platform weight of 5 kg and manipulated platform principle inertia elements of 0.06, 0.02 and 0.07 kgm^2, the eigenfrequencies were calculated. The minimum, maximum and average lowest resonance frequency of the telescopic version of the PKM in the entire workspace and in the best 70% of the workspace are listed in Table 4.

	Min	**Max**	**Average**
Telescopic: entire workspace	29.37	109.46	93.64
Telescopic: best 70% workspace	93.58	109.46	100.10

Table 4: Lowest resonance frequencies with a telescopic link in arm 1 for Gantry-Tau PKM.

7. Optimization of the manipulator work space

Work space optimization was made using a fully geometric approach. The benefit of a geometric approach is that it is much faster and more accurate than numerical solutions based on manipulator kinematics. The starting point for the geometric work space calculations was to study the cross-sectional work space in the YZ-plane as illustrated in Fig. 10 (left), where the circles are obtained by rotations of the arms. The centres of the circles are located at the linear actuators and the radii of the circles equal the projected arm lengths plus the distance from the end of the arms to the TCP. The solid lines in the figure indicate the positions of the support framework, which are not allowed to be surpassed by the TCP. The valid TCP positions are found in the darker cross sectional area in the figure. This area (A_{Total}) was calculated as a sum of sub areas according to: $A_{Total} = A_1 + A_2 + A_3 + A_4$.

The sub areas were in turn calculated by smaller areas as exemplified for the area A_3 in Fig. 10 (right). Q_1 is the depth and Q_2 is the height of the manipulator framework and the goal is to optimise the work space volume with respect to the design parameters Q_1, Q_2, L_1, L_2 and L_3, where L_i are the arm lengths. The sub area A_3 consists of two segments of a circle for small values of Q_2 because the upper limit of the workspace is partly circular and partly a straight line. At bigger values of Q_2 the upper limit will be the circle arc between the points (Q_1; Z_{3Q1}) and (Y_{13}; Z_{13}).

When the expressions for the cross sectional areas were obtained the next step was to calculate the workspace volume as a function of the cross-sectional areas. Fig. 11 shows the work space in the XZ-plane, which can be divided into 3 sections, sections 1 and 3 outside the guide ways and section 2 in between the guide ways. For sections 1 and 2, the cross sectional areas depend on the x-position while they are constant in section 2.

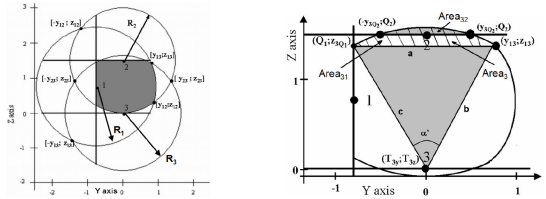

Figure 10: (Left): The cross-sectional workspace area of the Gantry-Tau in the YZ-plane. (Right): Example showing how to calculate the cross sectional Sub Area 3 (A_3)

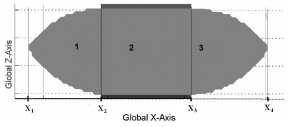

Figure 11: The workspace area of the Gantry-Tau machine in the XZ-plane when it is reconfigured to work in both positive and negative x-directions.

With the expressions obtained for the work space volume, a work space optimization problem was formulated as follows:

$$\max\ V(Q_1, Q_2, L_1, L_2, L_3) \qquad (10)$$
$$subject\ \ to\ \ Q_1 > 0,\ Q_2 > 0 \qquad L_1 > 0,\ L_2 > 0,\ L_3 > 0 \qquad V_U(Q_1, Q_2, L_1, L_2, L_3) = 0$$

With 2m length of the guide ways and with the manipulated platform dimensions used in the prototype manipulator at UiA the optimization resulted in the following design parameters: $Q_1 = 0.6426$ m; $Q_2 = 0.9947$ m; $L_1 = 0.9987$ m; $L_2 = 1.1101$ m; $L_3 = 0.9350$ m giving the work space volume: $V = 3.4687$ m^3. The installation space of the Gantry-Tau equals $(X_3 - X_2)Q_1Q_2$ which is 1.2783m^3 for the optimised

design. Hence, the total workspace to installation space ratio for the optimised design is 2.7135 which is very large for a PKM compared to most other PKMs which typically have a ratio of less than one.

8. Conclusions

The overview presented in this paper shows that the reconfigurable Gantry-Tau manipulator is a useful research platform as well as a promising structure with respect to the performance that can be obtained. It has been shown possible to make analytical inverse kinematics calculations for a 5 DOF version of the manipulator, a version that also can be used to make singularity free reconfiguration possible in order to increase the work space significantly. Using a geometric approach this enlarged work space can be optimized in a short time resulting in a manipulator design with a work space to footprint ration as high as 2.7. In order to find the TCP path for singularity free reconfiguration the link forces have been used to get a measure of the distances from singularities. The same link force calculations have also been used for the elastostatic performance calculations of the manipulator indicating high stiffness values at TCP. For the same design also the elastodynamics has been analysed using mass-spring models of the arm links and also in this case high performance will be possible to obtain.

References

[1] Johannesson, L. Berbyuk, V., Brogårdh, T: Gantry-Tau Robot – A New 3 Degrees of Freedom Parallel Kinematic Robot, Proc. 2nd Mechatronics Meeting, Sept 2003, Chalmers, Sweden.

[2] Abramowitz, M., Stegun, I. A., "Solutions of Quartic Equations." §3.8.3 in Handbook of Math. Functions with Formulas, Graphs, and Math. Tables, 9th ed, Dover, pp. 17-18, 1972.

[3] Borwein, P., Erdélyi, T., 1995, "Quartic Equations." §1.1.E.1e in Polynomials and Polynomial Inequalities. New York: Springer-Verlag, p. 4, 1995.

[4] I. Williams, G. Hovland, T. Brogårdh, "Kinematic Error Calibration of the Gantry-Tau Parallel Manipulator", Proc. of the IEEE Intl. Conf. on Rob. and Autom., Orlando, May 2006.

[5] C. Gosselin, "Stiffness Mapping for Parallel Manipulators", IEEE Trans. on Robotics and Automation, Vol. 6, No. 3, pp. 377-382, 1990.

[6] A. Schrijver, "Theory of Linear and Integer Programming", John Wiley & sons, 1998

[7] A. Bemporad, M. Morari, "Control of Systems Integrating Logic, Dynamics and Constraints", Automatica, No. 35, Vol. 3, pp. 407-427, 1999.

[8] C. Budde, P. Last, J. Hesselbach, "Workspace Enlargement of a Triglide Robot by Changing Working and Assembly Mode", Proc. IASTED Intl. Conf. Rob., pp. 244-248, Oct. 2005.

[9] M. Murray, G. Hovland, T. Brogårdh, "Collision-Free Workspace Design of the 5-Axis Gantry-Tau Parallel Kinematic Machine", Proc. IEEE/RSJ Conf. Intl. Robots, pp.2150-55, Oct 2006.

[10] I. Tyapin, G. Hovland, T. Brogårdh, "A Geometrical Method for Calculating the Unreachable Workspace of the 3-DOF Gantry-Tau Parallel Manipulator", Proc. of the Australasian Conf. on Robotics and Automation, Brisbane, Dec. 2007.